How to cite: *Angew. Chem. Int. Ed.* **2024**, *63*, e202405047
doi.org/10.1002/anie.202405047

Polymer Chemistry

Easy Synthetic Access to High-Melting Sulfurated Copolymers and their Self-Assembling Diblock Copolymers from Phenylisothiocyanate and Oxetane

*Jenny Stephan, Jorge L. Olmedo-Martínez, Christoph Fornacon-Wood, Merlin R. Stühler, Mathias Dimde, Daniel Braatz, Robert Langer, Alejandro J. Müller, Holger Schmalz, and Alex J. Plajer**

Abstract: Although sulfurated polymers promise unique properties, their controlled synthesis, particularly when it comes to complex and functional architectures, remains challenging. Here, we show that the copolymerization of oxetane and phenyl isothiocyanate selectively yields polythioimidocarbonates as a new class of sulfur containing polymers, with narrow molecular weight distributions (M_n = 5–80 kg/mol with $Đ \leq 1.2$; $M_{n,max}$ = 124 kg/mol) and high melting points of up to 181 °C. The method tolerates different substituent patterns on both the oxetane and the isothiocyanate. Self-nucleation experiments reveal that π-stacking of phenyl substituents, the presence of unsubstituted polymer backbones, and the kinetically controlled linkage selectivity are key factors in maximising melting points. The increased tolerance to macro-chain transfer agents and the controlled propagation allows the synthesis of double crystalline and amphiphilic diblock copolymers, which can be assembled into micellar- and worm-like structures with amorphous cores in water. In contrast, crystallization driven self-assembly in ethanol gives cylindrical micelles or platelets.

Introduction

Sulfur-containing polymers can exhibit improved semi-crystallinity, recyclability and degradability in comparison to their all-oxygen-containing counterparts, as well as unique properties such as high refractive indices rendering them, for example, as useful components in optical applications.[1–14] In this regard ring-opening copolymerization (ROCOP) of a strained heterocycle with a heteroallene such as carbon disulfide (CS_2), carbonyl sulfide (COS), or isothiocyanates (RNCS) can provide access to sulfur-containing polymers, which are otherwise difficult to obtain with common synthetic strategies.[15] Much work has focused on the copolymerization of substituted epoxides to produce polythiocarbonates.[16–27] However, these polymers are amorphous if the tacticity of the resulting stereocenter is not controlled. In contrast, unsubstituted epoxides, namely ethylene oxide, can lead to semi-crystalline materials in the ROCOP with sulfurated comonomers, as in this case, no tacticity control is required.[28,29] The disadvantage is, however, that ethylene oxide is an explosive and highly toxic gas requiring special reaction set-ups, which limits its applicability in standard research laboratories. In contrast, the unsubstituted four-membered analogue, trimethylene oxide, also known as oxetane (OX), is a liquid at ambient conditions and can also lead to unsubstituted semi-crystalline polymers. For example, copolymerization of OX with

[*] J. Stephan, M. R. Stühler, Dr. M. Dimde, Dr. D. Braatz
Institute for Chemistry and Biochemistry
Free University Berlin
Fabeckstraße 34/36, 14195 Berlin, Germany

Dr. J. L. Olmedo-Martínez, Prof. Dr. A. J. Müller
Department of Polymers and Advanced Materials, Physics, Chemistry and Technology, Faculty of Chemistry
University of the Basque Country UPV/EHU
Paseo Manuel de Lardizabal 3, 20018 Donostia-San Sebastián, Spain

C. Fornacon-Wood, Dr. H. Schmalz, Jun.-Prof. Dr. A. J. Plajer
Macromolecular Chemistry
University of Bayreuth
Universitätsstraße 30, 95447 Bayreuth, Germany
E-mail: alex.plajer@uni-bayreuth.de

Prof. Dr. R. Langer
Institute for Chemistry
Martin-Luther-University Halle-Wittenberg
Kurt-Mothes-Straße 2, 06120 Halle, Germany

Prof. Dr. A. J. Müller
IKERBASQUE, Basque Foundation for Science
Plaza Euskadi 5, 48009 Bilbao, Spain

Dr. H. Schmalz
Bavarian Polymer Institute (BPI)
University of Bayreuth
Universitätsstraße 30, 95447 Bayreuth, Germany

COS yields poly(trimethylene monothiocarbonate) with a melting temperature (T_m) of 128 °C.[30] Overcoming the practical challenge of using gaseous COS, our group and the group of Zhang recently reported the selective ROCOP of OX with liquid CS_2 which gave rise to poly(trimethylene dithiocarbonate) with a T_m of 82–89 °C.[31,32] However, both ROCOP reactions result in polymers with a broadened molecular weight distribution ($Đ > 1.5$) which is also observed for many other ring-opening polymerisations of sulfurated monomers.[33–39] This suggests the occurrence of side reactions alongside chain propagation, such as chain-end coupling and transesterification.[40] These side-reactions can reduce the resulting molecular weights, and can complicate the application of the polymerisations in the synthesis of more complex architectures, such as block copolymers. The latter would allow to rationally combine the properties of established polymers, such as poly(ethylene glycol) (PEG), with those of sulfurated ones. The improved semi-crystallinity of sulfurated polymers suggests their usefulness in applications requiring spatially confined crystallization, such as crystallization driven self-assembly (CDSA).[41,42] However, apart from poly(ethylene sulfide), sulfurated polymers have not yet been applied in this field, which is perhaps due to the challenging synthesis of the required amphiphilic block copolymers.[43,44] Here, we report the copolymerisation of phenylisothiocyanate (PhNCS) with OX granting a straightforward synthetic access to sulfurated polymers with high melting points and low dispersities as well as amphiphilic diblock copolymers that can be applied in CDSA.

Results and Discussion

To achieve the copolymerisation of PhNCS and OX we employed our recently developed heterobimetallic Cr(III)Rb catalyst (LCrRb) combining a Cr(III)OAc with a RbOAc active site, which has performed well with other sulfurated monomers (see Figure 1(a) and Supporting Information Section S1).[31,45] The ROCOP of 1 eq. LCrRb : 1000 eq. OX: 1000 eq. PhNCS at 80 °C (Table 1 run #1) produces a solid reaction mixture after 60 min. NMR spectroscopic analysis of the crude mixture (see Supporting Information Figure S7) shows three broadened resonances in the aliphatic CH_2 region of the spectrum at around 4.3, 2.9 and 2.0 ppm, in addition to the two sharp resonances assignable to unreacted OX at 4.8 and 2.7 ppm. The observation of three distinct CH_2 resonances is indicative of the ring-opening of the OX with the sulfur-containing comonomer, generating unsymmetrically substituted $(CH_2)_3$ units (i.e. –O–CH_2–CH_2–CH_2–S–). The absence of any additional sharp resonances in the crude NMR spectrum other than residual monomer indicates selective polymer formation. The polymer can be straightforwardly isolated from the unreacted monomers by precipitation, followed by drying of the solid under reduced pressure. The NMR spectroscopic analysis of the precipitated polymer (see Figure 1(b) and Supporting Information Figure S8, S9) indicates the equimolar incorporation of PhNCS and OX. The observation of a resonance at 157 ppm in the $^{13}C\{^1H\}$ NMR spectrum is in line with the formation of a heterocarbonate (see resonance 1 in Figure 1(b)), corresponding to a polymer with –$(CH_2)_3$–O–C(=NPh)–S– linkages (abbreviated as ONS).[34] The formation of a –C=N– group is further supported by IR spectroscopy with a characteristic band for the C–N-stretching vibration at $\tilde{\nu} = 1630\ cm^{-1}$ (see Figure 1(c)). In addition, small aliphatic ester

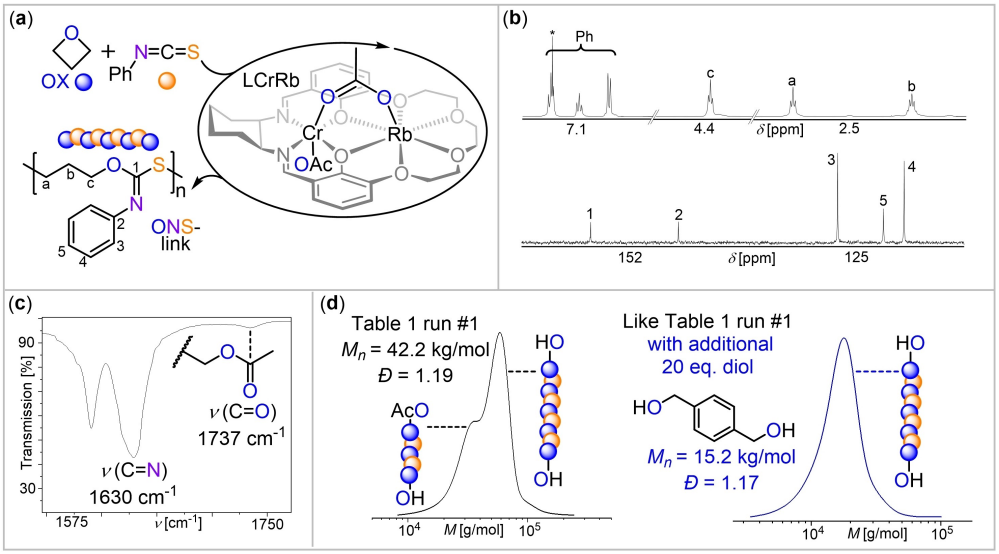

Figure 1. (a) PhNCS/OX ROCOP Scheme. (b) ^1H and ^{13}C NMR (*$CDCl_3$) of the copolymer corresponding to Table 1 run #1. (c) IR spectrum of the copolymer corresponding to Table 1 run #8. (d) Overlaid GPC traces of (black) copolymer corresponding to Table 1 run #1 and (blue) copolymer obtained from an analogous run to Table 1 run #1 with additional 20 eq. 1,4-benzenedimethanol acting as a bifunctional chain-transfer agent.

Table 1: PhNCS/OX copolymerization.

Run	Catalyst	Cat:PhNCS:OX	T [°C]	t [h]	TOF[a]	Pol. Select. [%][b]	ONS Select. [%][c]	$M_{n,\,app}$ [kg/mol] ($Đ$)[d]
#1	LCrRb	1:1000:1000	80	1	920	>99%	95	42.2 (1.19)
#2	LCrNa	1:1000:1000	80	8	180	>99%	78	19.4 (1.20)
#3	LCrK	1:1000:1000	80	7	150	>99%	87	39.0 (1.16)
#4	LZnK	1:1000:1000	80	24	–	–	–	–
#5	LCrRb	1:1000:1000	100	0.3	3300	>99%	91	28.0 (1.24)
#6	LCrRb	1:1000:500	80	1	1500	>99%	94	31.7 (1.16)
#7	LCrRb	1:2000:2200	80	2	n.d.	>99%	95	80.4 (1.20)
#8	LCrRb	1:8000:8200	80	24	n.d.	>99%	95	124.0 (1.70)
#9	LCrRb	1:50:50	80	1	n.d	>99%	95	4.6 (1.18)

[a] Turnover frequency (TOF) determined from fitting to the initial linear region of the conversion versus time plot obtained by ^{1}H NMR analysis of aliquots. [b] Relative integral in the normalised ^{1}H NMR spectrum of resonances from polymer versus small molecule by-products. [c] Relative integral in the normalised ^{1}H NMR spectrum of deconvoluted resonances from ONS repeat units versus OSN repeat units. [d] Apparent number averaged molecular weight determined by GPC (gel permeation chromatography) measurements conducted in THF, using narrow polystyrene standards to calibrate the instrument.

bands ($\tilde{\nu}$ = 1737 cm^{-1A}, see Figure 1(c)) are observed in the IR spectrum. These ester groups are formed via initiation by the acetate coligands in LCrRb inserting into OX. GPC analysis of the isolated polymer (see Figure 1(d) black trace) reveals a bimodal molecular weight distribution with M_n = 42.2 kg/mol ($Đ$ = 1.19). The chromatogram consists of two narrow overlapping distributions, centered at 30 kg/mol and 60 kg/mol, respectively. These findings suggest the presence of two distinct initiation events followed by highly controlled propagation steps.[31] End-group analysis by the ^{31}P-test also unambiguously shows the formation of alcohol chain ends (see Supporting Information Figure S16).[46] Hence the formation of α-OAc,ω-OH functional chains can be assumed.

However, the observed apparent molecular weight by GPC is somewhat lower than the theoretical molecular weight ($M_{n,theo}$ = 170 kg/mol) and we infer that chain-transfer reactions with bifunctional protic impurities (typically diols or H_2O) in the monomers are responsible for this. These act as bifunctional initiators that lead to the formation of α, ω-OH telechelic chains, which is furthermore supported by the weight difference of the overlapping distributions. Accordingly, we deliberately added an excess of a bifunctional alcohol (1,4-benzenedimethanol, 20 eq. per LCrRb) to a polymerisation reaction with otherwise analogous loadings as described in Table 1 run #1. This leads to a reduction of the obtained molecular weight to M_n = 15.2 kg/mol as well as an apparently monomodal molecular weight distribution with a slightly lower dispersity ($Đ$ = 1.17), as now α,ω-OH telechelic chains dominate the sample (Figure 1(d) blue trace). Importantly, these results show that propagation during PhNCS/OX ROCOP is very controlled as multimodality arises from different initiation processes.

The ^{1}H NMR spectrum of the PhNCS/OX copolymer encompasses a second minor set of resonances. These resonances are associated with a ^{13}C resonance at 188 ppm (Figure 2(a)) that can be assigned to thionourethane –$(CH_2)_3$–O–C(=S)–NPh– groups (OSN link).[47] Formation of both ONS and OSN links can be rationalised by a propagation mechanism as depicted in Figure 2(b). In this mechanistic scenario the alkoxide-bound intermediate **A**, formed after OX ring-opening, reacts with PhNCS to a κ^2-N,S coordinated thioimidocarbonate species **C** (ii). The subsequent ring-opening of the OX monomer can proceed via an attack of the sulfur atom in **C** (step (i)), leading to an ONS link, or via attack of the nitrogen atom in **C** (step (i)),

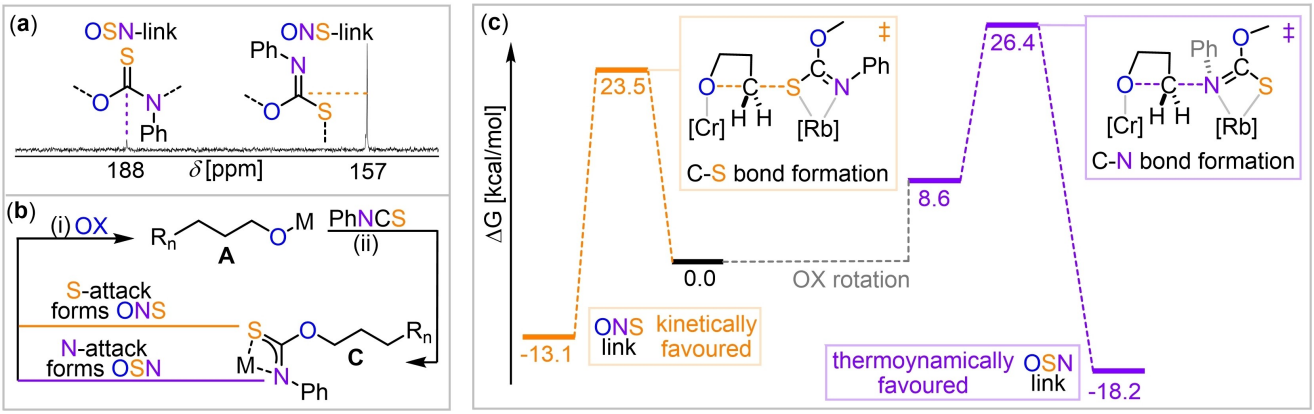

Figure 2. (a) Zoom into the ^{13}C NMR corresponding to Table 1 run #3. (b) Propagation steps leading to ONS and OSN links; M denotes metal catalyst, R_n denotes polymer chain. (c) Computed free energy profile of step (ii) on the ωB97XD/def2-TZVPP level of theory.

which generates an OSN link. To investigate which energetic factors govern the preferential formation of ONS links during propagation, we turned to DFT modelling on the ωB97XD/def2-TZVPP level of theory (see Figure 2(c) and Supporting Information Section S12). The assumed structure of **C** in which the chain end is coordinated in proximity to the incoming OX monomer was chosen in reference to related heteroallene copolymerisations of bimetallic catalysts.[21,48] Here, chain end coordination occurs at the alkali metal while OX activation occurs at the adjacent Cr(III) centre on the same side of the catalyst plane. Geometry optimization of a model for **C** with an additional coordinated OX monomer allowed for the localisation of two discrete minima. In those the heterocarbonate group at the chain-end and OX either arrange in a coplanar ($\Delta G = 8.6$ kcal/mol) or an almost perpendicular fashion ($\Delta G = 0.0$ kcal/mol). The perpendicular arrangement allows for a S_N2-type nucleophilic attack via the sulfur to form an ONS link, which is associated with an activation barrier of $\Delta G^{\ddagger} = 23.5$ kcal/mol (see Figure 2(c) orange path). In contrast, the attack via the nitrogen atom to form an OSN link requires rotation of the coordinated OX to allow for a S_N2-type nucleophilic attack of the nitrogen with a barrier of $\Delta G^{\ddagger} = 26.4$ kcal/mol (see Figure 2(c) purple path). In terms of insertion thermodynamics, the resulting product has a formation energy of −18.1 kcal/mol in the OSN and −13.1 kcal/mol in the ONS case. This suggests that the predominantly observed formation of the ONS link occurs due to kinetic rather than thermodynamic reaction control.

Next, we studied the effects of catalyst choice, monomer loading and reaction temperature. Changing the alkali metal from Rb (TOF 920 h^{-1}, 95 % ONS links, Table 1 run #1) to Na (TOF 180 h^{-1}, 78 % ONS links, Table 1 run #2) or K (TOF 150 h^{-1}, 87 % ONS links, Table 1 run #3) leads to a substantial decrease of the reaction rate as well as more OSN links. Unfortunately, the Cs derivative of LCrRb was not synthetically accessible. Changing the transition metal to Zn (Table 1 run #4) leads to a complete loss of activity. This demonstrates that the right combination of metals is crucial for both activity and selectivity which clearly indicates metal-metal cooperativity. Hence, we continued our studies with LCrRb. Moving from 80 to 100 °C (Table 1 run #5) leads to an approximate tripling of the rate to a high TOF of 3300 h^{-1} while somewhat reducing molecular weights. Deviating from the 1:1 PhNCS:OX ratio (Table 1 run #6) maintains rates and selectivity. Decreasing the catalyst loading expectedly increases molecular weights to $M_n = 80.4$ ($Đ = 1.20$, Table 1 run #6) and 124.0 kg/mol ($Đ = 1.70$, Table 1 run #7). Increasing the catalyst loading decreases molecular weights to $M_n = 4.6$ kg/mol ($Đ = 1.18$, Table 1 run #8) demonstrating that PhNCS/OX ROCOP allows to access of a wide range of molecular weights.

Wide angle X-ray scattering (WAXS) analysis of the as-synthesised PhNCS/OX copolymer of Table 1 run #1 (see Supporting Information Figure S21) shows distinct peaks at $2\theta = 16.0$, 19.0, 22.1 and 22.4° indicating semi-crystallinity ($X_c = 52$ %). Accordingly, differential scanning calorimetry (DSC) at a heating rate of 10 °C/min shows a complex multimodal endotherm associated with the melting of crystals (see Figure 3(a) 'First Heating') with the most pronounced peak at $T_m = 176$ °C. This is one of the highest melting points reported to date for ROCOP copolymers without tacticity control and is far above the T_m of many recently developed sulfur-containing polymers.[3,49–54] Similar melting points for this class of copolymers have only been achieved where molecular weights are limited ($M_n < 20$ kg/mol) or are not controllable due to e.g. side reactions or zwitterionic propagation pathways.[29,55–57] Interestingly, this sample does not crystallize upon cooling from the melt state in the calorimeter at 10 °C/min. The cooling and second heating scan presented in Figure 3(a) only display glass transitions and this is also true for slower cooling rates of 5 and 1 °C/min. Although the as-synthesised PhNCS/OX copolymer is semi-crystalline, its crystallisation from the melt is slow. Therefore, we designed a procedure to investigate if self-nucleation could induce crystallisation and prove the slow non-isothermal crystallisation kinetics of the material aiming for a generally applicable tool for the study

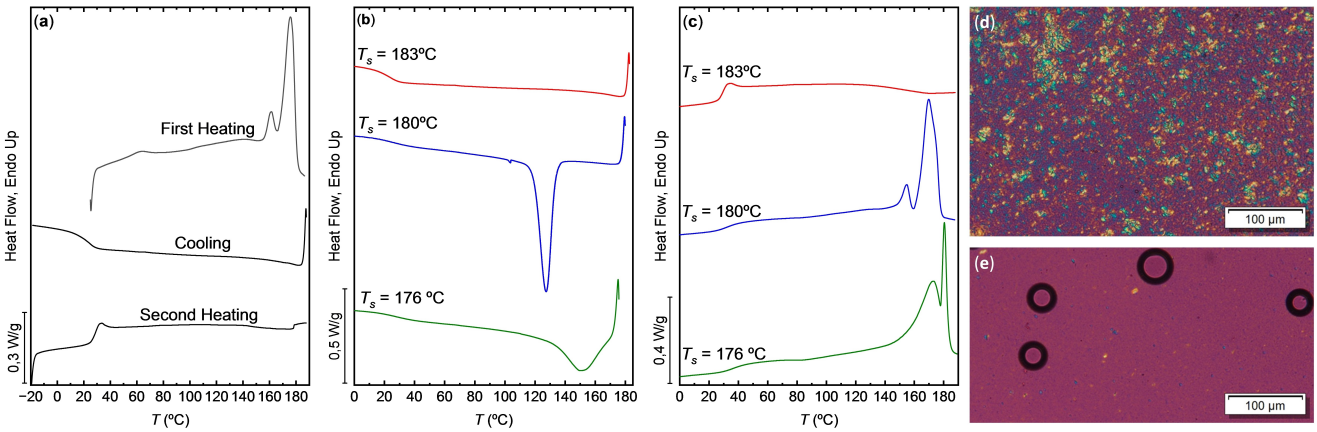

Figure 3. (a) DSC measurements of the polymer sample corresponding to Table 1 run #1. (b) First cooling from selected T_s temperatures and (c) subsequent heating after cooling from T_s. Polarized optical microscopy images of recrystallised polymers after annealing for 2 days at room temperature corresponding to (d) Table 1 run #1 and (e) Table 1 run #3; round objects surrounded by thick black edges are air bubbles.

of sulfurated polymers showing slow crystallisation.[32,49,58] To achieve self-nucleation (see Supporting Information Section S1) an as-synthesised polymer is heated to a specific temperature T_s whereafter the sample remains at T_s for 3 minutes before it is cooled. This specific time was chosen to saturate the self-nucleation effect while avoiding the risk of any sample degradation. Depending on T_s, three self-nucleation domains can be defined as follows. When T_s is higher than the end of the melting regime all crystals present in the sample are molten (*Domain I*, color code: red in Figure 3(b) and Figure 3(c)). All crystalline thermal history is erased, and the sample is not able to crystallise during cooling. When T_s is high enough to melt most of the crystals but low enough to leave some self-nuclei, self-nucleation occurs (*Domain II*, color code: blue in Figure 3(b) and Figure 3(c)). In this domain the melt is not isotropic and it either contains small crystal fragments (self-seeds) or the chains retain some of the conformational order they had in the crystals (self-nuclei). Upon cooling from T_s in *Domain II*, the sample crystallises due to self-nucleation, a crystallisation peak (T_c) is observed during cooling and the second DSC melting trace does not change significantly from the first. Finally, at lower T_s *Domain III* is entered (color code: green in Figure 3(b) and Figure 3(c)). The sample only partially melts, and the unmolten crystals anneal during the 3 min at T_s. Upon cooling from T_s, the sample crystallises at a higher T_c value because of the self-seeding effect of the unmolten crystals. In the second heating scan, an additional endothermic peak at a higher temperature is observed due to the melting of the annealed crystals. Figure 3(b) shows cooling scans from the indicated T_s values for the polymer from Table 1 run #1, while Figure 3(c) shows the subsequent heating scans. At T_s = 183 °C (*Domain I*), the sample is completely molten; any melt memory has been erased, and crystallization is prevented. At T_s = 180 °C (*Domain II*), the sample is efficiently self-nucleated, and crystallises with a clear and sharp crystallisation exotherm at T_c = 127 °C during cooling. At 176 °C (*Domain III*), T_s falls within the melting range of the material, causing partial melting. The unmolten crystals anneal during the 3 min at T_s and melt in the second heating cycle with a sharp peak at T_m = 181 °C. Polarized Light Optical Microscopy (PLOM) reveals that the crystals formed during cooling could not be observed by the limiting resolution imposed by the wavelength of visible light. However, after annealing the samples at room temperature for 2 days, crystalline superstructures were able to grow, and their microcrystalline texture of small superstructural aggregates was revealed, as seen in Figure 3(d). To investigate how linkage selectivity affects semi-crystallinity, DSC and PLOM were also performed with the sample from Table 1 run #3, which has a similar M_n but less chain regularity (87 % ONS-links). Although the as-synthesised sample is also semi-crystalline to the same extent as the one from run #1 by WAXS (X_c = 53 %), the dominant melting peak in the first heating scan is ca. 10 °C lower (T_m = 165 °C, see Supporting Information Figure S29). Likewise, after self-nucleation, it crystallises and melts at lower temperatures than the run #1 and forms much smaller crystalline aggregates (see Figure 3(e)).

Intrigued by the semi-crystallinity of the polymers we investigated the copolymerisation of other isothiocyanates and OX (see Figure 4(a)). The as-synthesised copolymers of OX with para-methyl (^{Me}PhNCS, Table 2 run #1) and para-fluoro (^{F}PhNCS, Table 2 run #2) substituted phenyl isothiocyanate show a smaller degree of semi-crystallinity indicated

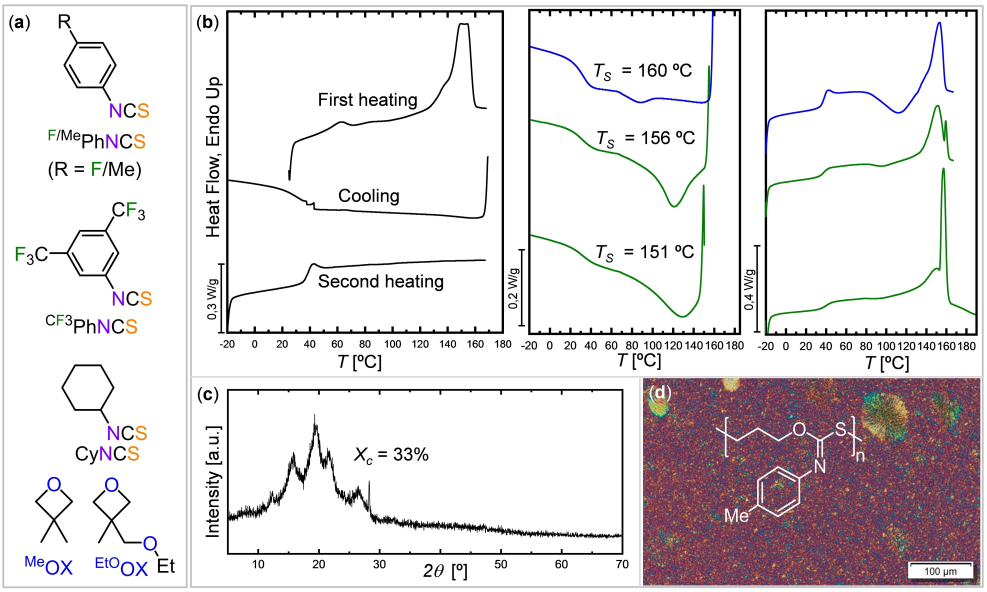

Figure 4. (a) Alternative oxetanes and isothiocyanates explored as part of the current study. (b) DSC measurements of the polymer sample corresponding to Table 2 run #1 (black traces) as well as first cooling and second heating scan (blue and green traces) from selected T_s temperatures. (c) WAXS spectrum of as-synthesised material (X_c = 33 %) and (d) PLOM images of recrystallised polymers corresponding to Table 2 run #1.

Table 2: Monomer scope.

Run	Monomers	t [h]	Conv. [%]	Pol. Select. [%][a]	ONS Select. [%][b]	$M_{n,\ app}$ [kg/mol] ($Đ$)[c]	T_m, T_g[d]	X_c [%][e]
#0	PhNCS/OX	1	92	>99	95	42.2 (1.19)	T_m = 176 °C; T_g = 28 °C	52
#1	^{Me}PhNCS/OX	2	82	>99	95	54.0 (1.17)	T_m = 151 °C; T_g = 38 °C	33
#2	^{F}PhNCS/OX	5	83	90	95	11.1 (1.50)	T_m = 154 °C; T_g = 23 °C	38
#3	^{CF3}PhNCS/OX	1	85	97	>99	77.3 (1.26)	T_m = 87 °C; T_g = 22 °C	14
#4	^{Cy}NCS/OX	20	90	65	95	25.9 (1.08)	T_g = 8 °C	–
#5	PhNCS/^{Me}OX	14	96	>99	81	47.0 (1.15)	T_m = 84 °C; T_g = 37 °C	30
#6	PhNCS/^{EtO}OX	21	77	>99	>99	34.6 (1.16)	T_g = 22 °C	–

Polymerisations conducted at 1 eq. LCrRb: 1000 eq. oxetane: 1000 eq. RNCS at 80 °C. [a] Relative integral in the normalised ^{1}H NMR spectrum of resonances from polymer versus small molecule by-products. [b] Relative integral in the normalised ^{1}H NMR spectrum of deconvoluted resonances from ONS repeat units versus other signals. [c] Apparent number averaged molecular weight determined by GPC (gel permeation chromatography) measurements conducted in THF, using narrow polystyrene standards to calibrate the instrument. [d] Melting point Tm determined from first heating scan of the as-synthesised polymer; glass transition temperature determined from the second cycle by differential scanning calorimetry. [e] Determined for the as-synthesised polymers by WAXS.

by WAXS analysis (X_c = 33 % for MePhNCS/OX and X_c = 38 % for FPhNCS/OX; see Figure 4(c) and Supporting Information Figure S39) and show lower melting points with respect to the unsubstituted derivative (T_m ca. 150 °C, see Figure 4(b) and Supporting Information Figure S38). They also rely on self-nucleation to crystallise during the non-isothermal DSC measurements, as exemplarily shown for the MePhNCS/OX copolymer for which spherulite formation could be resolved by PLOM after recrystallisation (Figure 4(d)). For the OX copolymer of 3,5-$(CF_3)_2$ substituted arylisothiocyanate (^{CF3}PhNCS, Table 2 run #4) an even lower melting point by DSC and degree of crystallinity by WAXS was observed (T_m ca. 87 °C, X_c = 14 %) and self-nucleation was not successful to crystallise the melt. The ROCOP of saturated cyclohexyl isothiocyanate (Table 2 run #4) with OX results in an amorphous polymer (T_g = 8 °C, see Supporting Information Figure S58). It becomes evident that increasing aryl substitution decreases the melting point while the absence of a π-system leads to an amorphous material, and we, therefore, infer that π-stacking interactions between the chains are at least partially responsible for the high T_m of the PhNCS/OX copolymer. Employing 3,3'-dimethyl substituted oxetane (^{Me}OX, Table 2 run #5) in combination with PhNCS yields a polymer that melts already at 84 °C (see Figure S66) and could also not be crystallised by self-nucleation. Accordingly, the as-synthesised polymer exhibits a lower crystallinity of X_c = 30 % by WAXS. This could again be due to the decreased ONS selectivity observed for PhNCS/^{Me}OX ROCOP. Though the methyl substituents on the backbone could also somewhat hinder the interaction of the phenyl rings between polymer chains. Moving to an unsymmetrically substituted oxetane bearing a methyl and a CH_2OEt substituent at the 3 position (^{EtO}OX, Table 2 run #6) yields an amorphous material with PhNCS presumably due to the atactic nature of the resulting polymer.

Having established the ROCOP of isothiocyanates and oxetanes as a robust methodology, we integrated this method in block copolymer synthesis. Since the copolymerisation tolerates alcohol chain transfer agents (see Figure 1-(d)), we hypothesized that the addition of alcohol-terminated polymers acting as macroinitiators could allow for the facile synthetic access to functional diblock copolymers. Hence, we added 20 equivalents of poly(ethylene glycol) monomethyl ether (i.e. Me-PEG-OH) to a copolymerisation reaction analogous to Table 1 run #1 (see Figure 5(a)) and obtained a polymer with a final apparent M_n of 8.0 kg/mol ($Đ$ = 1.01) after precipitation of the crude mixture. Diblock copolymer formation is clearly indicated by the increase in apparent molecular weight compared to the Me-PEG-OH macroinitiator before ROCOP (see Supporting Information Figure S80). ^{1}H NMR spectroscopy shows an approximate ratio of the PEG to PhNCS-*co*-OX of 3 to 1 (see Supporting Information Figure S76). Assuming a degree of polymerisation of 133 for the PEG block (as specified by the supplier), the degree of polymerisation for the PhNCS-*co*-

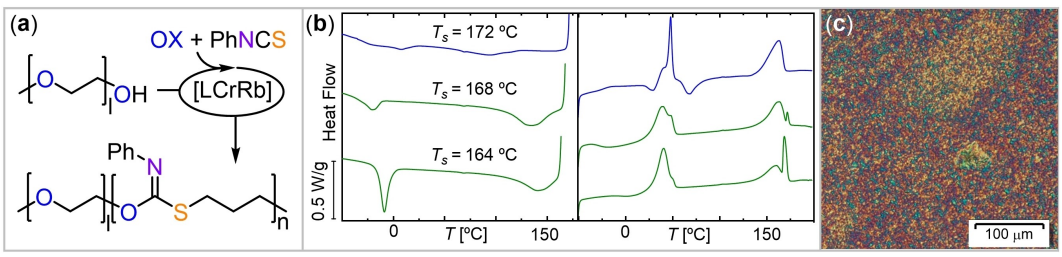

Figure 5. (a) PEG-*b*-(PhNCS-*co*-OX) synthesised by macro chain transfer strategy. (b) First cooling from the indicated T_s temperatures and subsequent second heating curve in DSC self-nucleation experiments for the diblock copolymer. (c) Polarised optical microscopy image of recycrystallised diblock copolymer.

OX block must be approximately 37. Note that some short acetate-initiated chains might have also formed alongside the Me-PEG-OH initiated chains, although the low dispersity indicates that the sample is primarily composed of the diblock copolymer after precipitation. DSC shows that the diblock copolymer features two distinct crystalline phases for the PEG and PhNCS-*co*-OX blocks respectively (see Figure 5(b)) with an overall crystallinity confirmed by WAXS of $X_c = 49\,\%$ (see Supporting Information Figure S82). Once again, self-nucleation is an effective way to induce crystallisation upon cooling from the appropriate T_s which could also be seen by PLOM (Figure 5(c)). As the PhNCS-*co*-OX block crystallises at higher temperatures from the self-nucleated melt (between 94 and 142 °C depending on T_s, see Figure 5(b) and Table S10), these crystals can nucleate the PEG block that crystallizes at much lower temperatures (between −21 and 9 °C). The lower the T_s, the higher the crystallinity of both blocks and, in particular, the PEG block, as concluded from the latent enthalpies of crystallisation reported in Table S10. Hence, the diblock copolymer has a clear tendency to self-assemble into distinct crystalline phases. As PEG and PhNCS-*co*-OX show different solubility properties, we hypothesized that the polymer may show tendencies for defined self-assembly. This is particularly interesting due to the slowly crystallising nature of the PhNCS-*co*-OX block offering a potential avenue to control the self-assembly process. Firstly, the self-assembly was investigated in water. For this purpose, the diblock copolymer was dissolved in 1,4-dioxane and then added dropwise into water under vigorous stirring. A cloudy but homogeneous solution was formed. Dynamic light scattering (DLS) experiments suggest the presence of nano-objects with an average size of 126 nm and a dispersity of 0.27 (see Supporting Information Figure S83). The DLS trace remains unchanged over multiple weeks highlighting the stability of the aggregates. Cryo transmission electron microscopy (cryo-TEM) reveals the formation of spherical aggregates with an average core-diameter of 29.6 ± 0.2 nm (Figure 6(a)). Furthermore, we also observed some elongated aggregates with an approximate length of 100–200 nm and a thickness of 10–30 nm, although there were too few for a statistical evaluation. As a single PhNCS-*co*-OX repeat unit in a stretched conformation extends across approximately 0.8 nm (see Supporting Information Figure S88), 37 repeat units extend across 30 nm at maximum. Therefore, the formation of micellar aggregates seems likely as the average core diameter of the objects observed falls within this range. The elongated aggregates consist of multiple merging micelles rather than regular cylindrical structures. This suggests that the cores are likely amorphous and not semi-crystalline, which we attribute to the slow crystallisation kinetics of PhNCS-*co*-OX. We hypothesized that moving to a weaker nonsolvent for the PhNCS-*co*-OX block in the self-assembly procedure and introducing an additional annealing step might provide sufficient time for core-crystallisation as the insoluble central block is precipitated less abruptly. This procedure has been previously used in CDSA of crystalline-coil diblock copolymers.[58–60] Hence, we repeated the self-assembly procedure outlined above

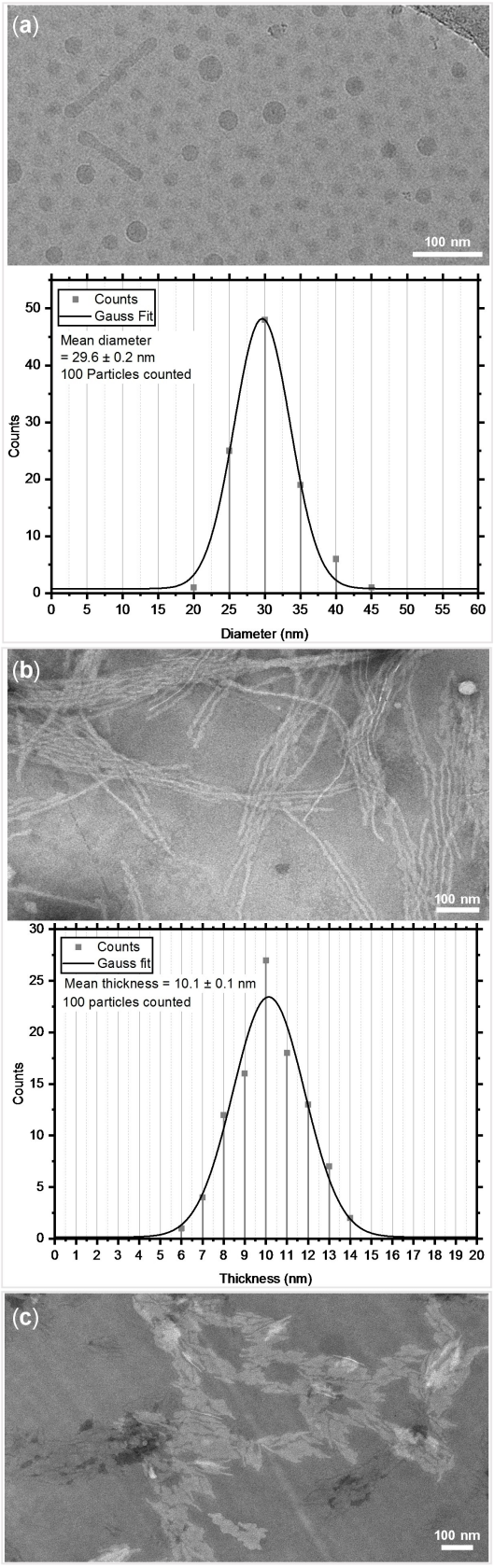

Figure 6. (a) Cryo-TEM image of spherical micellar aggregates obtained via aqueous nanoprecipitation and statistical evaluation of the mean diameter. (b) TEM images of cylindrical micelles and statistical evaluation of the mean thickness and (c) TEM images of platelets.

with ethanol in place of water as the nonsolvent for the crystallisable PhNCS-*co*-OX block followed by heating of the resulting solution at 80 °C for 1 day. A turbid solution that exhibits no sedimentation over the course of weeks was observed. TEM reveals the formation of uniform cylindrical micelles exceeding lengths of 500 nm (Figure 6(b)) and their regular shape contrasts the shorter irregular worm-like aggregates previously obtained in water. Stiff cylindrical micelles are typical objects obtained by CDSA, thus pointing to crystallisation as driving force for self-assembly in ethanol. The cylinders possess narrowly distributed thicknesses between 6 and 14 nm with a statistical average of 10.1 ± 0.1 nm, this points towards folding of the PhNCS-*co*-OX block within their cores. Heating the solution for another three days at 80 °C results in a different morphology as apparent from a shift of the average diameter by DLS from 170 to 770 nm (see Supporting Information Figure S84 and S85). TEM reveals the fusion of the cylinders to platelets (see Figure 6(c)). Similar platelets can also be obtained by sonication of the bulk material followed by annealing (see Supporting Information Figure S87) although further investigations of sulfur-containing polymers in CDSA are required.

Conclusion

In conclusion, we have established the copolymerisation of oxetanes (OX) with isothiocyanates (PhNCS) as a practical method to obtain sulfurated copolymers. The method can deliver materials with high molecular weights that exhibit some of the highest melting points in the field. To study their crystallisation, we developed a self-nucleation procedure revealing kinetically governed linkage selectivity, as well as phenyl substitution, to be key for maximizing crystallinity. Demonstrating the utility of the new polymerisation, we have prepared an amphiphilic and double-crystalline diblock copolymer for which the crystallisation of one block seeds the crystallisation of the other. Because of the crystallisation kinetics, nanostructures with different morphologies due to amorphous (spherical and worm-like aggregates) or semi-crystalline cores (cylindrical micelles and platelets) can be obtained depending on the self-assembly conditions. Owing to the degradability and recyclability benefits that sulfurated polymers can exhibit, PhNCS-*co*-OX holds potential as an alternative to established thermoplastic polymers.

Acknowledgements

AJP would like to acknowledge the VCI for a Liebig Fellowship as well as the assistance of the Core Facility BioSupraMol. AJM and JLOM would like to acknowledge funding by the Basque Government through grant IT1503-22. Open Access funding enabled and organized by Projekt DEAL.

Conflict of Interest

The authors declare no conflict of interest.

Data Availability Statement

The data that support the findings of this study are available in the supplementary material of this article.

Keywords: sulfur containg polymer · ring-opening polymerisation · semi-crystalline polymers · polymerisation catalysis

[1] T.-J. Yue, W.-M. Ren, X.-B. Lu, *Chem. Rev.* **2023**, *24*, 14038–14083.
[2] J. Jia, J. Liu, Z.-Q. Wang, T. Liu, P. Yan, X.-Q. Gong, C. Zhao, L. Chen, C. Miao, W. Zhao, S. (Diana) Cai, X.-C. Wang, A. I. Cooper, X. Wu, T. Hasell, Z.-J. Quan, *Nat. Chem.* **2022**, *14*, 1249–1257.
[3] Y. Wang, M. Li, J. Chen, Y. Tao, X. Wang, *Angew. Chem. Int. Ed.* **2021**, *60*, 22547–22553.
[4] T.-J. Yue, B.-H. Ren, W.-J. Zhang, X.-B. Lu, W.-M. Ren, D. J. Darensbourg, *Angew. Chem. Int. Ed.* **2021**, *60*, 4315–4321.
[5] J. Zhang, T. Bai, W. Liu, M. Li, Q. Zang, C. Ye, J. Z. Sun, Y. Shi, J. Ling, A. Qin, B. Z. Tang, *Nat. Commun.* **2023**, *14*, 3524.
[6] Y.-L. Su, L. Yue, H. Tran, M. Xu, A. Engler, R. Ramprasad, H. J. Qi, W. R. Gutekunst, *J. Am. Chem. Soc.* **2023**, *25*, 13950–13956.
[7] Y. Xia, X. Yue, Y. Sun, C. Zhang, X. Zhang, *Angew. Chem. Int. Ed.* **2023**, *62*, e202219251.
[8] F. H. Sobotta, M. T. Kuchenbrod, F. V. Gruschwitz, G. Festag, P. Bellstedt, S. Hoeppener, J. C. Brendel, *Angew. Chem. Int. Ed.* **2021**, *60*, 24716–24723.
[9] J. Zhang, Q. Zang, F. Yang, H. Zhang, J. Z. Sun, B. Z. Tang, *J. Am. Chem. Soc.* **2021**, *143*, 3944–3950.
[10] J. Peng, T. Tian, S. Xu, R. Hu, B. Z. Tang, *J. Am. Chem. Soc.* **2023**, *145*, 28204–28215.
[11] T. Tian, R. Hu, B. Z. Tang, *J. Am. Chem. Soc.* **2018**, *140*, 6156–6163.
[12] J. J. Griebel, S. Namnabat, E. T. Kim, R. Himmelhuber, D. H. Moronta, W. J. Chung, A. G. Simmonds, K.-J. Kim, J. van der Laan, N. A. Nguyen, E. L. Dereniak, M. E. Mackay, K. Char, R. S. Glass, R. A. Norwood, J. Pyun, *Adv. Mater.* **2014**, *26*, 3014–3018.
[13] D. H. Kim, W. Jang, K. Choi, J. S. Choi, J. Pyun, J. Lim, K. Char, S. G. Im, *Sci. Adv.* **2020**, *6*, eabb5320.
[14] C. Shi, M. L. McGraw, Z.-C. Li, L. Cavallo, L. Falivene, E. Y.-X. Chen, *Sci. Adv.* **2020**, *6*, eabc0495.
[15] A. J. Plajer, C. K. Williams, *Angew. Chem. Int. Ed.* **2022**, *61*, e202104495.
[16] X.-F. Zhu, R. Xie, G.-W. Yang, X.-Y. Lu, G.-P. Wu, *ACS Macro Lett.* **2021**, *10*, 135–140.
[17] X.-F. Zhu, G.-W. Yang, R. Xie, G.-P. Wu, *Angew. Chem. Int. Ed.* **2022**, *61*, e202115189.
[18] X.-F. Zhu, X.-Y. Lu, C.-K. Xu, Y.-B. Fang, G.-W. Yang, W. Li, J. Wang, G.-P. Wu, *Chin. J. Chem.* **2023**, *41*, 3311–3318.
[19] D. Silbernagl, H. Sturm, A. J. Plajer, *Polym. Chem.* **2022**, *13*, 3981–3985.
[20] P. Deglmann, S. Machleit, C. Gallizioli, S. M. Rupf, A. J. Plajer, *Catal. Sci. Technol.* **2023**, *13*, 2937–2945.
[21] J. Stephan, M. R. Stühler, S. M. Rupf, S. Neale, A. J. Plajer, *Cell Rep. Phys. Sci.* **2023**, 101510.

[22] X. Geng, Z. Liu, C. Zhang, X. Zhang, *Macromolecules* **2023**, *56*, 4649–4657.
[23] C.-J. Zhang, T.-C. Zhu, X.-H. Cao, X. Hong, X.-H. Zhang, *J. Am. Chem. Soc.* **2019**, *141*, 5490–5496.
[24] D. K. Tran, A. N. Braaksma, A. M. Andras, S. K. Boopathi, D. J. Darensbourg, K. L. Wooley, *J. Am. Chem. Soc.* **2023**, *145*, 18560–18567.
[25] M. Sengoden, G. A. Bhat, D. J. Darensbourg, *Green Chem.* **2022**, *24*, 2535–2541.
[26] T.-J. Yue, W.-M. Ren, L. Chen, G.-G. Gu, Y. Liu, X.-B. Lu, *Angew. Chem. Int. Ed.* **2018**, *57*, 12670–12674.
[27] K. Nakano, G. Tatsumi, K. Nozaki, *J. Am. Chem. Soc.* **2007**, *129*, 15116–15117.
[28] W.-M. Ren, T.-J. Yue, M.-R. Li, Z.-Q. Wan, X.-B. Lu, *Macromolecules* **2017**, *50*, 63–68.
[29] J.-L. Yang, Y. Wang, X.-H. Cao, C.-J. Zhang, Z. Chen, X.-H. Zhang, *Macromol. Rapid Commun.* **2021**, *42*, 2000472.
[30] H.-L. Wu, J.-L. Yang, M. Luo, R.-Y. Wang, J.-T. Xu, B.-Y. Du, X.-H. Zhang, D. J. Darensbourg, *Macromolecules* **2016**, *49*, 8863–8868.
[31] C. Fornacon-Wood, B. R. Manjunatha, M. R. Stühler, C. Gallizioli, C. Müller, P. Pröhm, A. J. Plajer, *Nat. Commun.* **2023**, *14*, 4525.
[32] G. Feng, X. Feng, X. Liu, W. Guo, C. Zhang, X. Zhang, *Macromolecules* **2023**, *56(17)*, 6798–6805.
[33] S. Rupf, P. Pröhm, A. J. Plajer, *Chem. Sci.* **2022**, *13*, 6355–6365.
[34] E. F. Clark, G. Kociok-Köhn, M. G. Davidson, A. Buchard, *Polym. Chem.* **2023**, *14*, 2838–2847.
[35] J. Diebler, H. Komber, L. Häußler, A. Lederer, T. Werner, *Macromolecules* **2016**, *49*, 4723–4731.
[36] C. Gallizioli, D. Battke, H. Schlaad, P. Deglmann, A. J. Plajer, *Angew. Chem. Int. Ed.* **2024**, e202319810.
[37] Y. Xiao, T.-J. Yue, B.-H. Ren, W.-M. Ren, X.-B. Lu, *ACS Catal.* **2023**, *13*, 16215–16221.
[38] E. M. López-Vidal, G. L. Gregory, G. Kociok-Köhn, A. Buchard, *Polym. Chem.* **2018**, *9*, 1577–1582.
[39] C. Hardy, G. Kociok-Köhn, A. Buchard, *Chem. Commun.* **2022**, *58*, 5463–5466.
[40] J. Xu, P. Zhang, Y. Yuan, N. Hadjichristidis, *Angew. Chem. Int. Ed.* **2023**, *62*, e2022188.
[41] L. MacFarlane, C. Zhao, J. Cai, H. Qiu, I. Manners, *Chem. Sci.* **2021**, *12*, 4661–4682.
[42] A. K. Pearce, T. R. Wilks, M. C. Arno, R. K. O'Reilly, *Nat. Chem. Rev.* **2021**, *5*, 21–45.
[43] E. Sevgen, M. Dolejsi, P. F. Nealey, J. A. Hubbell, J. J. de Pablo, *Macromolecules* **2018**, *51*, 9538–9546.
[44] C. E. Brubaker, D. Velluto, D. Demurtas, E. A. Phelps, J. A. Hubbell, *ACS Nano* **2015**, *9*, 6872–6881.
[45] C. Fornacon-Wood, M. R. Stühler, C. Gallizioli, B. R. Manjunatha, V. Wachtendorf, B. Schartel, A. J. Plajer, *Chem. Commun.* **2023**, *59*, 11353–11356.
[46] A. Spyros, D. S. Argyropoulos, R. H. Marchessault, *Macromolecules* **1997**, *30*, 327–329.
[47] J. Yang, L. Zhen, L. Jiang, *ChemistrySelect* **2019**, *4*, 6177–6180.
[48] A. C. Deacy, A. Phanopoulos, W. Lindeboom, A. Buchard, C. K. Williams, *J. Am. Chem. Soc.* **2022**, *144*, 17929–17938.
[49] Y. Wang, Y. Zhu, W. Lv, X. Wang, Y. Tao, *J. Am. Chem. Soc.* **2023**, *145*, 1877–1885.
[50] Y. Zhu, M. Li, Y. Wang, X. Wang, Y. Tao, *Angew. Chem. Int. Ed.* **2023**, *62*, e202302898.
[51] Y. Xia, P. Yuan, Y. Zhang, Y. Sun, M. Hong, *Angew. Chem. Int. Ed.* **2023**, *62*, e202217812.
[52] P. Yuan, Y. Sun, X. Xu, Y. Luo, M. Hong, *Nat. Chem.* **2022**, *14*, 294–303.
[53] T. Sehn, B. Huber, J. Fanelli, H. Mutlu, *Polym. Chem.* **2022**, *13*, 5965–5973.
[54] Y. Zhu, Y. Tao, *Angew. Chem. Int. Ed.* **2024**, *63*, e2023173.
[55] K. Soga, I. Hattori, M. Sato, S. Ikeda, *J. Polym. Sci.* **1979**, *17*, 215–224.
[56] D. Tan, X. Hu, Z. Cao, M. Luo, D. J. Darensbourg, *ACS Macro Lett.* **2020**, *9*, 866–871.
[57] H. Yokota, M. Kondo, *J. Polym. Sci.* **1971**, *9*, 13–25.
[58] M. Inam, G. Cambridge, A. Pitto-Barry, Z. P. L. Laker, N. R. Wilson, R. T. Mathers, A. P. Dove, R. K. O'Reilly, *Chem. Sci.* **2017**, *8*, 4223–4230.
[59] Y. Kwon, K. T. Kim, *Macromolecules* **2021**, *54*, 10487–10498.
[60] J. Jiang, E. Nikbin, G. Hicks, S. Song, Y. Liu, E. C. N. Wong, I. Manners, J. Y. Howe, M. A. Winnik, *J. Am. Chem. Soc.* **2023**, *145*, 1247–1261.

Manuscript received: March 13, 2024
Accepted manuscript online: March 23, 2024
Version of record online: April 23, 2024